International Journal of Pharmaceutics: X 9 (2025) 100316

Contents lists available at ScienceDirect

International Journal of Pharmaceutics: X

journal homepage: www.sciencedirect.com/journal/international-journal-of-pharmaceutics-x

Topical transdermal administration of lenalidomide nanosuspensions-based hydrogels against melanoma: In vitro and in vivo studies

Mengdi Zhang [1], Haiying Qiu [1], Zheyi Han, Yazhong Ma, Jingjing Hou, Jingwei Yuan, Haiyan Jia, Menglu Zhou, Hongjie Lu, Yan Wu [*]

Air Force Medical Center, PLA, Air Force Medical University, Beijing, China.

ARTICLE INFO

Keywords:
Lenalidomide nanosuspensions-based hydrogels
Transdermal administration
Melanoma Transcriptomic
Immunoregulation

ABSTRACT

Percutaneous neoadjuvant therapy has proven effective in diminishing tumor size and the surgical intervention area, which couldeffectively mitigate the risk of tumor recurrence and enhance immunotherapy efficacy. Lenalidomide, an approved medication orally used to treat myeloma, was loaded into nanosuspensions-based hydrogels (Len-NBHs) for transdermal administration as a percutaneous neoadjuvant therapy. This study was designed to investigate the inhibitory effect and mechanism of Len-NBHs on melanoma. Network pharmacology and transcriptomic analyses identified key targets and signaling pathways. The effects of lenalidomide on melanoma were further verified through Western blotting, immunohistochemistry, immunofluorescence, and quantitative real-time polymerase chain reaction , using both in vitro cell experiments and in vivo melanoma mouse models. Lenalidomide could induce melanoma cells apoptosis, disrupt cell cycle progression, impede cell migration and invasion, and modify tumor microenvironment (TME). Mechanistically, lenalidomide reversed the abnormal activation of the PI3K-AKT signaling pathway and the overexpression of CD93, while also recruiting CD8+ T cells, CD4+ T cells, and dendritic cells to infiltrate the tumor site. Transdermal administration of Len-NBHs represents a promising adjuvant therapy for the treatment of malignant melanoma. Preoperative administration of Len-NBHs can inhibit the outward spread of melanoma, reduce tumor size, thereby decreasing the surgical excision area and improving patient survival rates and prognosis.

1. Introduction

In the last decade, the incidence of malignant melanoma has exhibited a concerning increase, marking it as one of the fastest-growing malignancies globally. This surge in cases has raised substantial health concerns, particularly due to the fact that patients diagnosed with metastatic melanoma typically experience poor prognosis, with an average survival period ranging from 6 to 10 months [Schadendorf et al., 2018; Gordon, 2013].

In the current landscape of melanoma treatment, surgical resection remains the primary approach and is often supplemented with adjuvant therapies like chemotherapy, radiotherapy and targeted immunotherapy. Nevertheless, approximately 30 % of melanoma patients have limited responsiveness to these therapeutic modalities, which can be partly attributed to the activation of specific tumor cell pathways conferring resistance to treatment. Additionally, the associated drug toxicity imposes a significant burden on the survival and overall well-being of individuals with malignant melanoma [Domingues et al., 2018; Hossain and Eccles, 2023; Carr et al., 2020; Patel et al., 2020; Davis et al., 2019] To address these challenges, the percutaneous administration of neoadjuvant therapy has been proposed as a promising approach to maximize the efficacy of melanoma treatment while concurrently minimizing adverse side effects [Chen et al., 2023]. Lenalidomide, with its immunoregulatory, anti-angiogenic, and anti-tumor properties, has shown promising effectiveness in this regard [Semeraro et al., 2013; Stewart, 2014; Fuchs, 2019]. Considering the distinctive attributes of malignant melanoma, including a high prevalence of mutant antigens and immunosuppressive features, researchers are exploring the potential of lenalidomide to inhibit tumor angiogenesis, restore immune homeostasis, suppress tumor growth, and activate diverse skin dendritic cell subsets in promoting a more robust immune response.

* Corresponding author at: Air Force Medical Center, PLA., No.30 Fucheng Road, Haidian District, Beijing 100142, China.
E-mail address: wuyan2023@fmmu.edu.cn (Y. Wu).
[1] These authors contributed equally to this work.

https://doi.org/10.1016/j.ijpx.2025.100316
Received 27 August 2024; Received in revised form 9 January 2025; Accepted 13 January 2025
Available online 16 January 2025

In this study, we developed a nanosuspensions hydrogel to improve the transdermal delivery of drugs for melanoma treatment. We combined nanosuspensions hydrogels with lenalidomide to design and prepare lenalidomide nanosuspensions-based hydrogels (Len-NBHs). Both in vitro and in vivo studies demonstrated that transdermal lenalidomide administration significantly inhibited the growth of subcutaneous tumors. Then, network pharmacology analysis, transcriptomic analysis and experimental validation were performed to elucidate the mechanism underlying this observed tumor growth inhibition, which supported that lenalidomide represent a promising new adjuvant therapy for percutaneous skin-related cancer. Preoperative administration of Len-NBHs can inhibit the outward spread of melanoma, reduce tumor size, thereby decreasing the surgical excision area and improving patient survival rates and prognosis.

2. Material and methods

2.1. Materials

Lenalidomide (purity ≥99 %) was purchased from Beijing Ouhe Technology Co., Ltd. Antibodies, including anti-AKT1, anti-pAKT1, anti-PI3K, anti-pPI3K, anti-MMP9, anti-MMP2, anti-TNFα, anti-EGFR, anti-CD93, anti-VEGFA, anti-CD4, anti-CD8, anti-CD86, anti-CD80, anti-CD11c, anti-β-actin, and goat anti-Rabbit IgG H&L / HRP antibody, were obtained from Proteintech Group, Inc. (Wuhan, China), and Beijing Biosynthesis Biotechnology Co. Matrigel and ECL ultrasensitive luminescence solution were bought from Shanghai Universal Biotech Co., Ltd. The CCK-8 kit and AO/EB kit were acquired from Wuhan Servicebio Technology Co., Ltd. DMEM medium and fetal bovine serum (FBS) were purchased from Thermo Fisher Biochemical Products (Beijing) Co., Ltd. The protein extraction kit and protein quantification kit were obtained from Beijing Solarbio Science & Technology Co., Ltd. RT mix with DNase and SYBR Green Supermix were procured from US Everbright® Inc. (Suzhou, China). ELISA kits were purchased from Shanghai Enzyme-linked Biotechnology Co., Ltd. Cell cycle and cell viability detection reagents were bought from Sino BioTool (Shanghai) Co., Ltd.

2.2. Animals

Seven-week-old female SPF C57BL mice (18–22 g) were obtained from Beijing Vital River Laboratory Animal Technology Co., Ltd. (License No.: SCXK 2021–0006). They were housed in individually ventilated cages under a 12-h light/dark cycle at a constant temperature of 24 ± 1 °C. They had free access to standard rodent feed and water. All experimental protocols with mice followed the ARRIVE guidelines (Animal Research: Reporting of In Vivo Experiments) and were approved by the Ethics Committee of the Air Force Medical Center (Ethical approval number: 2023–31-PJ01).

2.3. Preparation of the lenalidomide nanosuspensions-based hydrogels

The lenalidomide nanosuspension was prepared by grinding with wet media. 300 mg hydroxypropyl cellulose (JF Pharm) and 150 mg sodium dodecyl sulfatewas were dissolved individually in 50 mL distilled water, then two groups of transparent solution were obtained. After mixing the two solutions at a volume ratio of 1:1, lenalidomide and 30 mL zirconia beads were added and ground for 14 h to obtain lenalidomide nanosuspensions (Len-Na). Finally, the lenalidomide nanosuspensions-based hydrogels (Len-NBHs) was made from 1 g carbomer swelling in Len-Na. Then Len-Na was prepared into freeze-dried powder to observe its morphology by scanning electron microscope (SEM). Drug loading content of Len-NBHs was consitently monitored by HPLC (SHIMADZU, Japan) [Hou et al., 2023].

2.4. In vitro drug permeation study

The skin used in the experiment was obtained from male ICR mice (weighing 22 ± 2 g, aged 6 weeks), provided by SPF Biotechnology Co., Ltd. (Beijing, China). In vitro release experiments were conducted using Franz diffusion cells with a diffusion area of 1.76 cm^2. The mouse skin was securely positioned between the donor and receptor chambers, with the receptor chamber containing 14.5 mL of PBS (pH 7.4), maintained at 37 °C with continuous stirring. Next, 0.5 g of Len-NBHs was applied to the surface of mouse skin. During the experiment, 1 mL of receptor solution (total volume 14.5 mL) was collected from the receptor chamber at 2, 4, 6, 8, 12, and 24 h, and an equal volume of preheated buffer solution (37 °C) was added to maintain in vitro permeation conditions. The concentration of lenalidomide in the extracted solution was analyzed using HPLC. The experiment was terminated after 24 h, and the skin was washed with 3 mL of pure water to remove residual Len-NBHs, dried with filter paper, and the portion of skin used for diffusion was preserved. The preserved skin was cut into small pieces, placed in 1 mL of methanol, and subjected to ultrasonic treatment for 60 min to ensure complete drug extraction. Finally, the supernatant was centrifuged at 15,000 rpm for 10 min and analyzed by HPLC. The drug content in the skin was calculated in micrograms per unit area of skin tissue. The experimental groups included 0.5 %, 1 %, 2 %, 3 %, and 4 % Len-NBHs (containing 0.5 g, 1 g, 2 g, 3 g, and 4 g of lenalidomide in 100 g of Len-NBHs, respectively). The control group consisted of a 1 % lenalidomide hydrogel (dispersing 1 g of lenalidomide raw material into 99 g of hydrogel).

2.5. Cell and lenalidomide preparation

B16-F10 cells were obtained from the Air Force Characteristic Medical Center Clinical Medicine Experiment Center (Beijing, China). These cells were cultured in DMEM supplemented with 10 % FBS, 1 % penicillin, and 1 % streptomycin. The cell cultures were maintained at 37 °C in an environment with 5 % CO_2. Lenalidomide was dissolved in DMSO and stored at −20 °C.

2.6. Network pharmacology analysis

We retrieved both the related and predicted targets of lenalidomide from various databases, including the SwissTargetPrediction, PharmMapper, DrugBank data, STITCH, SEA, SuperPRED, and ChEMBL database [Daina et al., 2019; Wang et al., 2017; Knox et al., 2024; Szklarczyk et al., 2016]. Additionally, the TTD, GeneCards, DisGeNET, OMIM, MalaCards, PharmGKB, and CTD database [Zhou et al., 2024; Stelzer et al., 2016; Piñero et al., 2020; Amberger et al., 2015; Rappaport et al., 2017; Whirl-Carrillo et al., 2021; Davis et al., 2023] were used to retrieve melanoma-related targets. Melanoma-related targets of lenalidomide were identified using the Venny online tool. Subsequently, we constructed a PPI network using data obtained from the STRING database [Szklarczyk et al., 2023] and GraphBio [Zhao and Wang, 2022]. The top 35 targets were used to create a heatmap using ImageGP [Chen et al., 2024]. GO enrichment analysis, and KEGG pathway enrichment analysis, were performed using the David database [Sherman et al., 2022]. Then, the top 15 GO terms and the top 35 KEGG pathways were selected for visualization and further analysis. Survival curves for the top 35 melanoma-related targets were constructed using data from the UALCAN database [Chandrashekar et al., 2022], with the *p*-value less than 0.05. Lenalidomide was subjected to molecular docking studies with core targets that are closely associated with patient survival. Molecular docking was conducted using Autodock [Eberhardt et al., 2021]. to assess the binding energy between lenalidomide and the macromolecular target proteins.

2.7. CCK-8 assay

B16-F10 cells in their logarithmic growth phase were seeded into 96-well plates at densities of 4×10^5 cells/well, 2×10^5 cells/well and 1×10^5 cells/well, and allowed to adhere overnight. Subsequently, the cells were exposed to lenalidomide at varying concentrations ranging from 0 to 30 μM. At 24, 48 and 72 h post-treatment, 10 μL of CCK-8 solution was added to each well, and the cells were further incubated for 1–4 h. The absorbance was measured at 450 nm using a microplate reader (BioTek, USA).

2.8. AO/EB dual staining assay, cell cycle and viability assay

B16-F10 cells in their logarithmic growth phase were seeded into 6-well plates at a density of 5×10^6 cells/well. After overnight incubation to ensure complete cell adherence, the cells were treated with lenalidomide for 24 h. AO/EB dual staining assay: the culture medium was removed, and the cells were washed twice with PBS. Subsequently, the cells were incubated with an acridine orange/ethidium bromide (AO/EB) solution at room temperature for 5–10 min. Images were then captured using a fluorescence microscope (Leica, Germany). Cell cycle and viability assay: specialized reagents for cell cycle and cell viability detection were added to the cells, and the tests were conducted after a specified incubation period using the NucleoCounter® NC-250™ (Denmark).

2.9. Colony formation assay, scarification test, and transwell invasion assays

B16-F10 cells were plated in 6-well plates at a density of 5000 cells/well and treated with lenalidomide for 72 h. In the absence of drugs, the cells were recultured for 7 days with medium changes every 3 days. After culture, the cells were fixed with 4 % paraformaldehyde for 20 min, followed by washing with PBS. Subsequently, they were incubated with a 0.1 % crystal violet solution for 20 min, washed with PBS, and photographed [Xi et al., 2022]. To assess cell migration, a scratch test was performed. Cells were seeded in 6-well plates and allowed to reach an appropriate density. A scratch was created using a 10 μL pipette tip, and the wells were washed with PBS to remove detached cells. Photographs were taken under a microscope (Zeiss, Germany). The cells were then treated with lenalidomide for 48 h, and photographs were captured again using the microscope. For invasion assays, the Transwell system was used. Cells were collected and resuspended in a serum-free medium containing lenalidomide at a concentration of 5×10^5 cells/mL. Subsequently, 100 μL of the cell suspension was placed in the upper chamber coated with Matrigel, while 500 μL of medium containing 20 % FBS was added to the lower chamber. After incubation for 24 h, the cells on the lower side of the upper chamber were fixed with 4 % paraformaldehyde, stained with 0.1 % crystal violet, washed with PBS, and photographed under a microscope.

2.10. Real-time quantitative PCR (RT-qPCR) analysis

Total RNA was extracted employing TRIzol reagent, followed by reverse transcription using RT mix with DNase. RT-qPCR was conducted using SYBR Green Supermix and a real-time PCR detection system (BIO-RAD, USA). GAPDH served as the internal control for normalization. The mRNA expression levels were determined using the $2^{-\Delta\Delta CT}$ method. Primer sequences for the target genes are shown in Table 1.

2.11. Tumor-bearing mouse model experiment

Thirty mice were randomly allocated into 5 groups, each comprising 6 mice: the control group, model group, and treatment groups including high-dose Len-NBHs (H-Len), medium-dose Len-NBHs (M-Len) and low-dose Len-NBHs (L-Len). Except for the mice of the control group, all the other mice were inoculated with 0.1 mL of B16-F10 cells (1×10^7 cells/mL) in the armpit to establish an allogeneic tumor transplantation model. On the third day following the B16-F10 cell injection, the treatment group received 0.5 g Len-NBHs via percutaneous administration (twice one day), while the model group and the control group were administered a blank substrate. Tumor diameters were measured, and tumor sizes were calculated using the formula: tumor volume = 1/2 × long diameter × (short diameter)^2. At the end of the treatment, the mice were humanely euthanized using pentobarbital sodium anesthesia. Tumor samples were collected, and serum was separated. Hematoxylin and eosin (H.E.) staining, pathological analysis, immunocytochemistry (IHC), immunofluorescence (IF), western blot analysis and transcriptomic analysis were performed on tumor samples and adjacent tissues. Related factors in serum were detected by ELISA kits.

Table 1
Primer sequences.

Gene symbol	Forward primer (5′–3′)	Reverse primer (5′–3′)
MMP9	GCAGAGGCATACTTGTACCG	TGATGTTATGATGGTCCCACTTG
MMP2	ACCTGAACACTTTCTATGGCTG	CTTCCGCATGGTCTCGATG
AKT1	TTCTCAGTGGCACAATGTCAG	TCCATCTCCTCAGCACCTG
PI3K	GATGAGGTGAGGAACGAAG	GCAGAGGACTTGTTGCC
GAPDH	TCCATCTCCTCAGCACCTG	TGGTCCAGGGTTTCTTACTCC

2.12. Statistical analysis

The results are presented as mean ± standard deviation. Statistical analysis was performed using GraphPad Prism 8.0, with one-way analysis of variance used to assess differences between data sets. The significance level of $P < 0.05$ were considered to be statistically significant.

3. Results

3.1. Lenalidomide nanosuspensions-based hydrogels

Lenalidomide was ground into a nanosuspension by wet medium grinding, so that it was mixed in the hydrogel with a smaller particle size to achieve better bioavailability. Fig. 1A and Fig. 1B showed the SEM images of lenalidomide and the Len-Na freeze-dried powder. The raw material drug of lenalidomide was irregularly crystalline, the particle size was in the micron level, and the size was uneven, while the Len-Na freeze-dried powder was uniform in size, uniform in distribution, and the particle size reached the nanometer level. We investigated the permeation effect of Len-NBHs through in vitro drug permeation experiments. As the drug concentration increased, the skin permeation rate of Len-NBHs gradually decreased, which may be related to the increased particle size and instability of the lenalidomide nanodispersion with increased drug concentration, leading to sedimentation and aggregation. The skin cumulative drug permeation rate (24 h) of Len-NBHs (0.5 %, 1 %, 2 %, 3 %, and 4 %) and lenalidomide (1 %) were 14.35 %, 12.07 %, 8.23 %, 3.93 %, 1.77 %, and 1.35 % respectively (Fig. 1C). The corresponding amounts of cumulative drug permeation per unit area (24 h) were 121.94 μg/cm^2, 237.62 μg/cm^2, 264.95 μg/cm^2, 200.13 μg/cm^2, 91.23 μg/cm^2, and 22.01 μg/cm^2 (Fig. 1D), while the drug deposition per unit area of skin (24 h) were 10.88 μg/cm^2, 10.99 μg/cm^2, 10.72 μg/cm^2, 10.89 μg/cm^2, 10.03 μg/cm^2, and 3.73 μg/cm^2 (Fig. 1E). The skin cumulative permeation rate, cumulative drug permeation, and drug deposition of Len-NBHs were all higher than those of lenalidomide, indicating that Len-NBHs can effectively enhance the rate of transdermal absorption of lenalidomide and increase its accumulation in the skin, forming a drug reservoir in the skin. Based on the experimental results, we selected 3 % Len-NBHs for the H-Len group, 2 % Len-NBHs for the M-Len group, and 1 % Len-NBHs for the L-Len group for subsequent *in vivo* experiments.

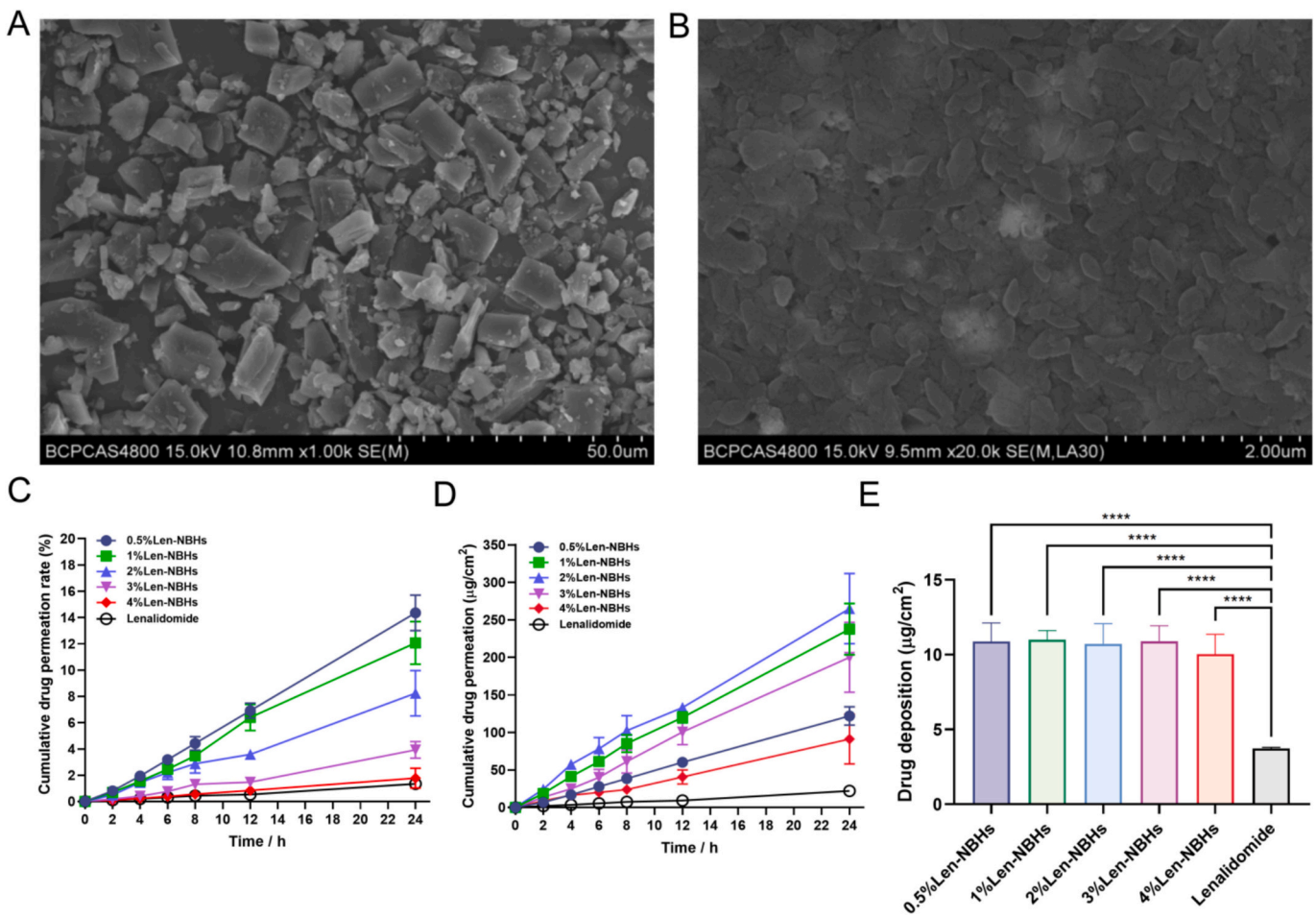

Fig. 1. Lenalidomide nanosuspensions-based hydrogels. (A) Morphology of lenalidomide by SEM. (B) Morphology of the Len-Na freeze-dried powder by SEM. (C) Cumulative lenalidomide permeation rate within 24 h. (D) Cumulative lenalidomide permeation within 24 h. (E) Lenalidomide deposition within 24 h.

3.2. Lenalidomide inhibited cell viability and proliferation and induced apoptosis of B16-F10 cells

The cell viability was determined using CCK-8 assay. Lenalidomide significantly decreased the viability of B16-F10 cells in a dose-dependent manner (Fig. 2A). The calculated IC_{50} value of lenalidomide in B16-F10 cells was approximately 4.52 μM. Consequently, for subsequent experiments, three different lenalidomide concentrations (1.25 μM, 2.5 μM, and 5 μM) were selected for treating the B16-F10 cells. In the cell colony formation assay, lenalidomide led to a marked, dose-dependent decrease in the number of cell colonies compared to untreated control cells (Fig. 2B), which confirmed the inhibitory effect of lenalidomide on melanoma cell. Following AO/EB double staining revealed the cell apoptosis rate after incubation with various concentration of lenalidomide. Intact cells emitted green fluorescence, whereas apoptotic cells emitted red fluorescence. Compared to the untreated control group, lenalidomide-treated cells exhibited an increase in red fluorescence, with fluorescence intensity rising in a dose-dependent manner, signifying an elevated number of apoptotic cells (Fig. 2C). Next, the cell apoptosis rate induced by lenalidomide was determined by VB-48/PI staining followed. VB-48 can be used as a marker for detection of mid- to late-stage apoptosis in mammalian cells as high levels of reduced thiols within any given cell will result in a high fluorescence intensity of VB-48. Compared to untreated control cells, lenalidomide led to a substantial dose-dependent increase in apoptosis among B16-F10 cells (Fig. 2D). Furthermore, cell cycle analysis revealed that lenalidomide arrested B16-F10 cells in the G0/G1 phase, as opposed to the untreated group, which resulted in the inhibition of cell proliferation (Fig. 2E).

3.3. Lenalidomide inhibited the migration and invasion of B16-F10 cells

In both the scratch test and the transwell experiment, the migration and invasion capabilities of cells in the treatment group were significantly reduced compared to untreated control cells (Fig. 3A, B), demonstrating the effective inhibitory effects of lenalidomide on the outward migration and invasion of melanoma cells. Matrix metalloproteinases (MMPs), including MMP-2 and MMP-9, are key enzymes in tumor-cell growth and invasion. We further investigated the expression of MMP-2 and MMP-9. The treatment group exhibited a significant decrease in the expression of MMP-2 and MMP-9 ($p < 0.001$, Fig. 3C, D), aligning with the observed inhibition of B16-F10 cell migration and invasion, as well as the induction of apoptosis. To further confirm the gene-regulatory effects of lenalidomide on melanoma, the relative mRNA expression of MMP-2 and MMP-9 significantly decreased in the treated groups compared to the untreated group ($p < 0.05$, Fig. 3E). This reduction in the high expression of these genes, which contribute to melanoma migration, invasion and proliferation, suggests that lenalidomide can reverse these effects.

3.4. High in vivo anti-melanoma activity of Len-NBHs

Mice bearing B16-F10 tumors were subjected to daily percutaneous treatments with Len-NBHs at different dose. The tumor in the three treatment groups shrinked significantly than the model group ($p < 0.001$, Fig. 4A, B), indicating an obvious in vivo anti-tumor effect of

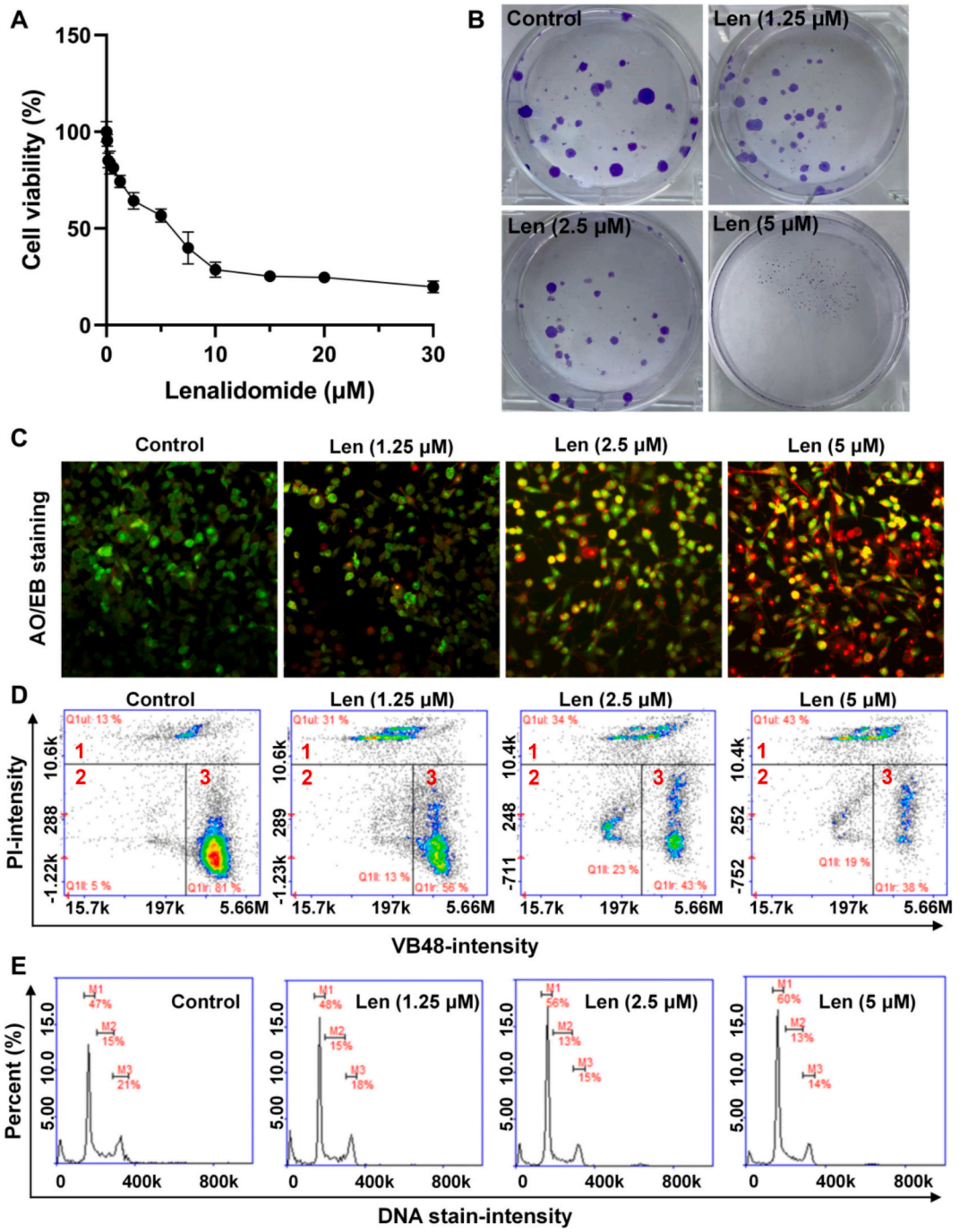

Fig. 2. In vitro inhibitory effect against B16-F10 cells of lenalidomide. (A) The viability of B16-F10 cells incubated with lenalidomide at concentrations ranging from 0 to 30 μM for 24 h. (B) Colony formation of B16-F10 cells incubated with lenalidomide at different concentrations (1.25, 2.5, 5 μM). (C) AO/EB dual staining images of B16-F10 cells incubated with lenalidomide at different concentrations (1.25, 2.5, 5 μM), scale bar = 50 μm. (D) cell viability of B16-F10 cells incubated with lenalidomide at different concentrations (1.25, 2.5, 5 μM), Part 1: Dead cells. Part 2: Low activity cells. Part 3: High activity cells. (E) Cell cycles of B16-F10 cells incubated with lenalidomide at different concentrations (1.25, 2.5, 5 μM).

lenalidomide. Interestingly, the experiments indicated that a higher concentration of Len-NBHs did not necessarily result in a more pronounced tumor inhibition effect. In fact, the inhibitory effect of H-Len on tumor growth was inferior to that of M-Len and L-Len, although no significant difference observed between M-Len and L-Len. Lenalidomide's immunomodulatory effect includes enhancing the number and activity of T cells and natural killer cells while inhibiting the release of inflammatory cytokines IL-4 and IL-6, and increasing the secretion of IL-2 and INF-γ [Hideshima et al., 2021; Hagner et al., 2017; Zhang et al., 2009; Marriott et al., 2002; Gandhi et al., 2014; Krämer et al., 2016]. In the present study, the cytokines including IL-4, IL-6, IL-2, and INF-γ were determined by using ELISA analysis. As expected, compared to the model group, all the three the treatment groups exhibited significantly lower IL-4 and IL-6 level ($p < 0.001$, Fig. 4C, D), meanwhile the IL-2 and INF-γ increased obviously ($p < 0.05$, Fig. 4E, F). Remarkably, the expression levels of Th1 markers IL-4, and IL-6 in the H-Len group were lower than those in the M-Len or L-Len groups ($p < 0.05$). Conversely, the expression levels of Th2 markers IL-2, and IFN-γ were higher in the H-Len group ($p < 0.001$). This discrepancy indicates that high doses of lenalidomide may lead to a Th1/Th2 immune response imbalance

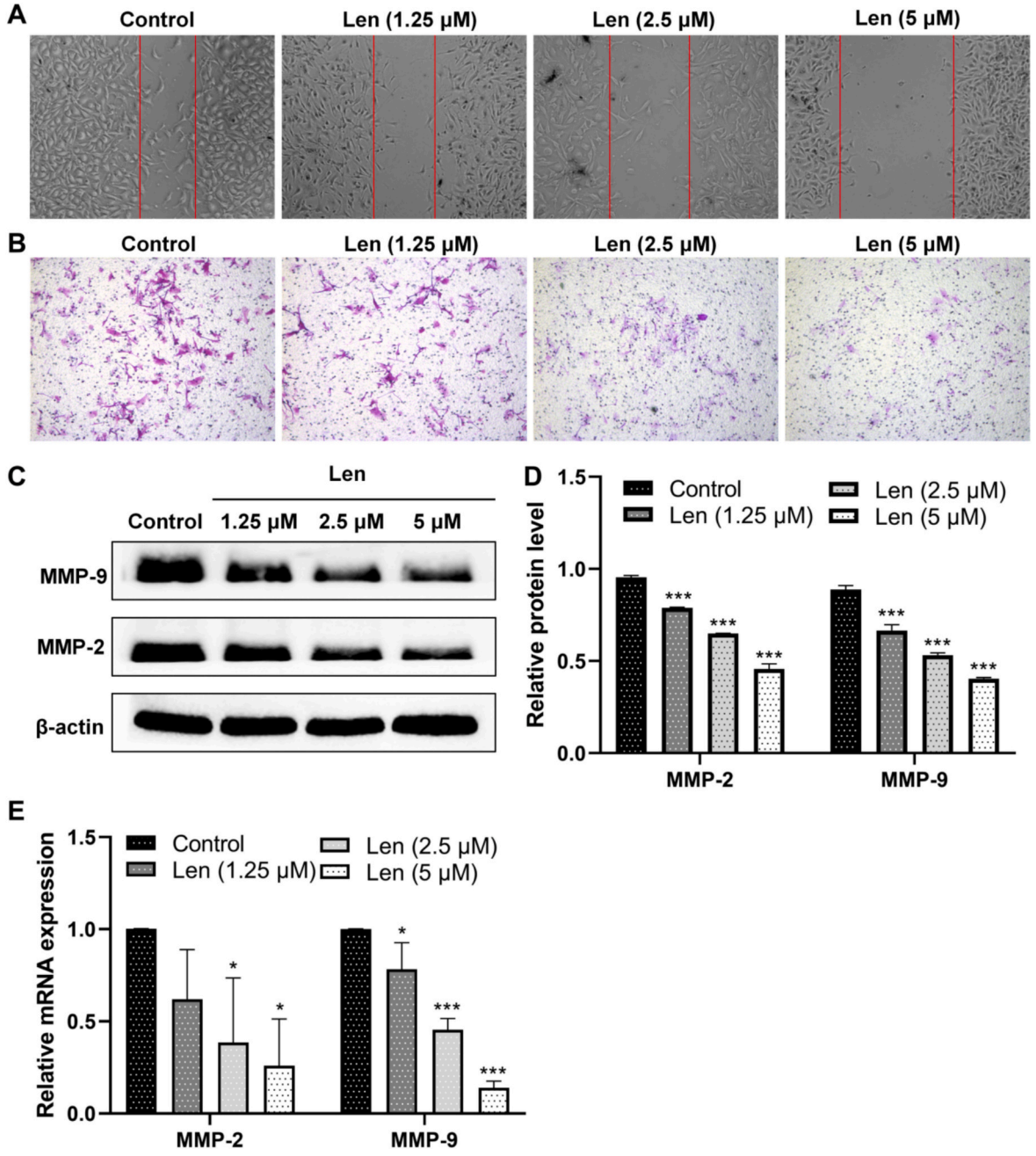

Fig. 3. Inhibition of B16-F10 cell migration and invasion by lenalidomide. (A) Scratch test of B16-F10 cells incubated with lenalidomide at different concentrations (1.25, 2.5, 5 μM). (B) Transwell assay of B16-F10 cells incubated with lenalidomide at different concentrations (1.25, 2.5, 5 μM). (C) Western blot assay of MMP-2 and MMP-9 expressed by B16-F10 cells incubated with lenalidomide at different concentrations (1.25, 2.5, 5 μM). (D) Quantitative analysis of MMP-2 and MMP-9 expression. (E) RT-qPCR analysis of the relative mRNA expression of MMP-2 and MMP-9 in B16-F10 cells incubated with lenalidomide at different concentrations (1.25, 2.5, 5 μM). $^{*}p < 0.05$, $^{***}p < 0.001$ vs the control group.

[Hetland et al., 2011], potentially weakening the effect of tumor growth inhibition. Similar findings were observed in another animal pharmacodynamic study of lenalidomide for psoriasis treatment [Jia et al., 2022], where H-Len demonstrated a weaker effect in improving skin lesions compared to the other two dose groups. Among the treatments, the 1 % Len-NBHs displayed the most significant therapeutic effect on tumors. Furthermore, Len-NBHs induced substantial damage to the tumor cell nucleus and extensive disruption of tumor tissue compared to model group (Fig. 4G).

Caner immunotherapy harnesses a patient's immune system to target cancer and has resulted in novel therapeutic approaches and unprecedented clinical outcomes. During the tumor specific immune response, tumor-defined T cells are activated when they encounter tumor antigens presented by antigen-presenting cells (APCs) such as dendritic cells (DCs). Mature DCs marked with CD80, CD86 and CD11c can drive the production of effector $CD4^{+}$ T helper 1 (Th1) and $CD8^{+}$ T cell-dominated immune responses. IHC and IF results (Fig. 5) indicated that Len-NBHs treatment led to an increase in the expression of CD80, CD86 and CD11c dendritic cell markers in the tumor area, along with increased expression of CD4 and CD8 T cell markers, suggesting enhanced infiltration of mature DCs and effective T lymphocytes within the tumor microenvironment.

Expressions of MMP-2, MMP-9 and VEGF are closely linked to growth, invasion, metastasis and angiogenesis of carcinoma. Compared

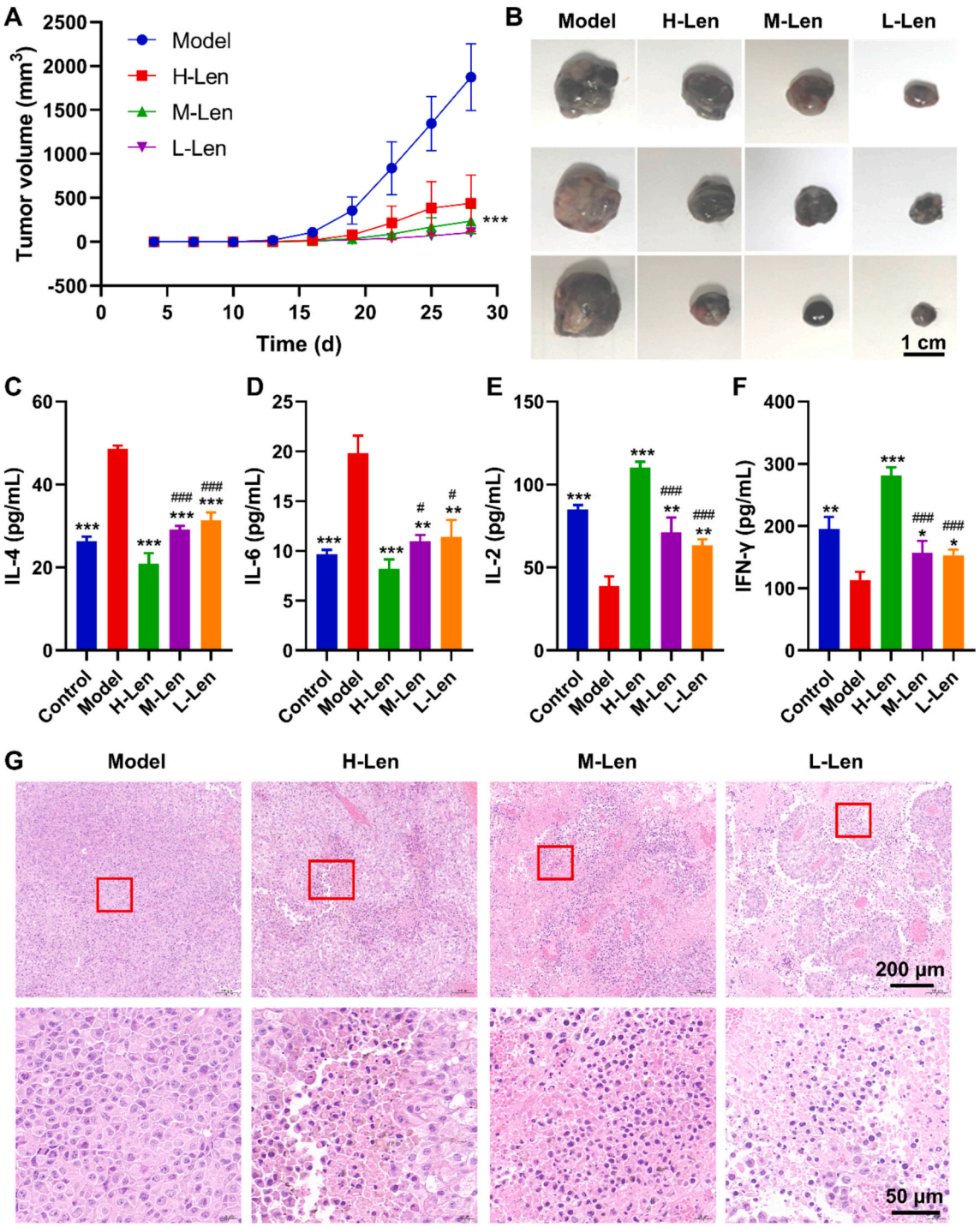

Fig. 4. In vivo anti-melanoma activity of trans-dermally administrated Len-NBHs. (A) Evolution of tumor volume during the experiment. (B) Pictures of excised tumor in different groups. (C) IL-4 levels in serum. (D) IL-6 levels in serum. (E) IL-2 levels in serum. (F) IFN-γ levels in serum. (G) HE staining images of tumor tissue, scale bar = 200 μm/50 μm. $^{*}p < 0.05$, $^{**}p < 0.01$, $^{***}p < 0.001$, vs the model group; $^{\#}p < 0.05$, $^{\#\#\#}p < 0.001$, vs the H-Len group.

to the untreated control group, Len-NBHs were effective in inhibiting the upregulation of MMP-2, MMP-9, EGFR, VEGFA and CD93 expression in tumor tissues (Fig. 6), suggesting Len-NBHs could influence tumor cell invasion and angiogenesis in tumor tissues, thereby inhibiting tumor growth.

3.5. Network pharmacology analysis

Having demonstrated the favorable immune and anti-tumor effects of lenalidomide against melanoma, we performed a multi-step series of investigations to implicate the mechanism responsible, beginning with network pharmacology analysis. We identified a total of 756 lenalidomide-related targets and 27,377 melanoma-related targets. After screening, they were narrowed down to 346 predicted targets for lenalidomide in melanoma (Fig. S1). A PPI network was constructed for these predicted targets (Fig. 7A), and we selected the top 35 target proteins based on their degree values (Table S1). These top 35 target proteins were further categorized into up-regulated and down-regulated groups ($|\text{LogFC}| > 2$) and visualized in a heatmap (Fig. S2). The analysis revealed that the 35 protein targets were associated with 395 GO

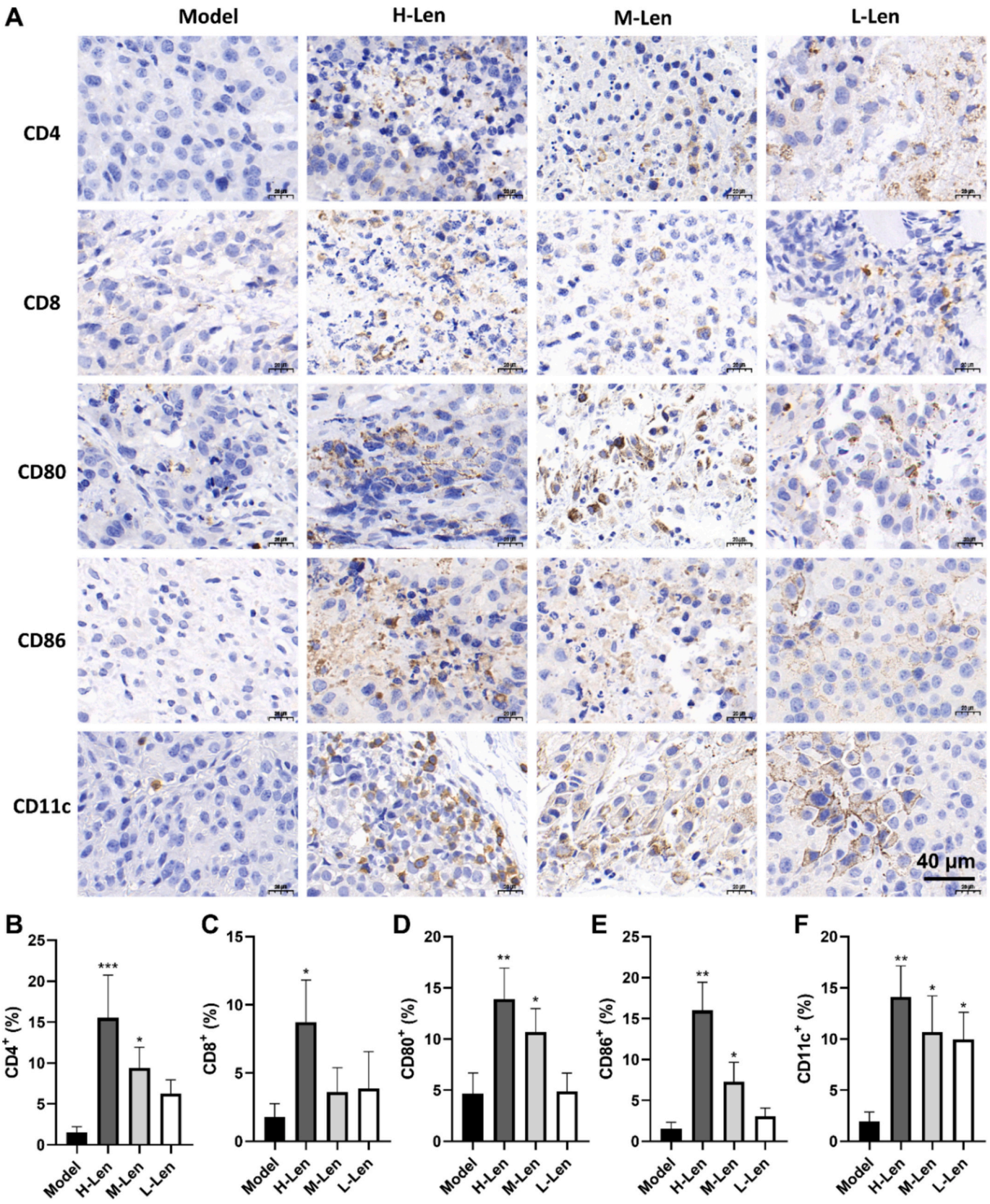

Fig. 5. Immune response in the tumor microenvironment. (A) The IHC images of CD4, CD8, CD80, CD86, and CD11c in different groups, scale bar = 40 μm. (B-F) Quantitative analysis of expression of CD4, CD8, CD80, CD86, and CD11c, respectively. *$p < 0.05$, **$p < 0.01$, ***$p < 0.001$, vs the model group.

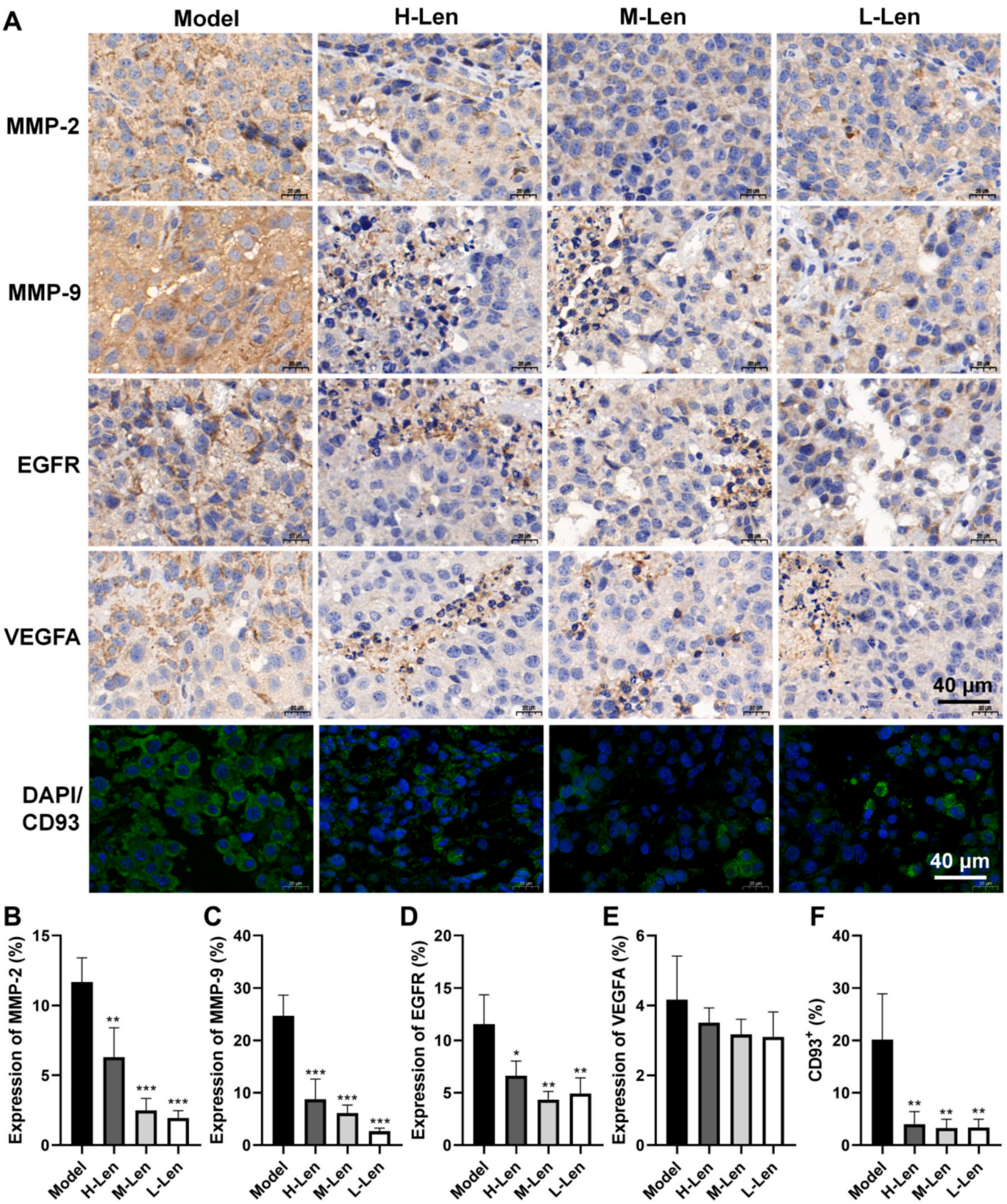

Fig. 6. Protein expression related to tumor invasion and angiogenesis. (A) The IHC images of MMP-2, MMP-9, EGFR, VEGFA and the merged IF images of DAPI and CD93, scale bar = 40 μm. (B-F) Quantitative analysis of expression of MMP-2, MMP-9, EGFR, VEGFA, and CD93, respectively. *$p < 0.05$, **$p < 0.01$, ***$p < 0.001$, vs the model group.

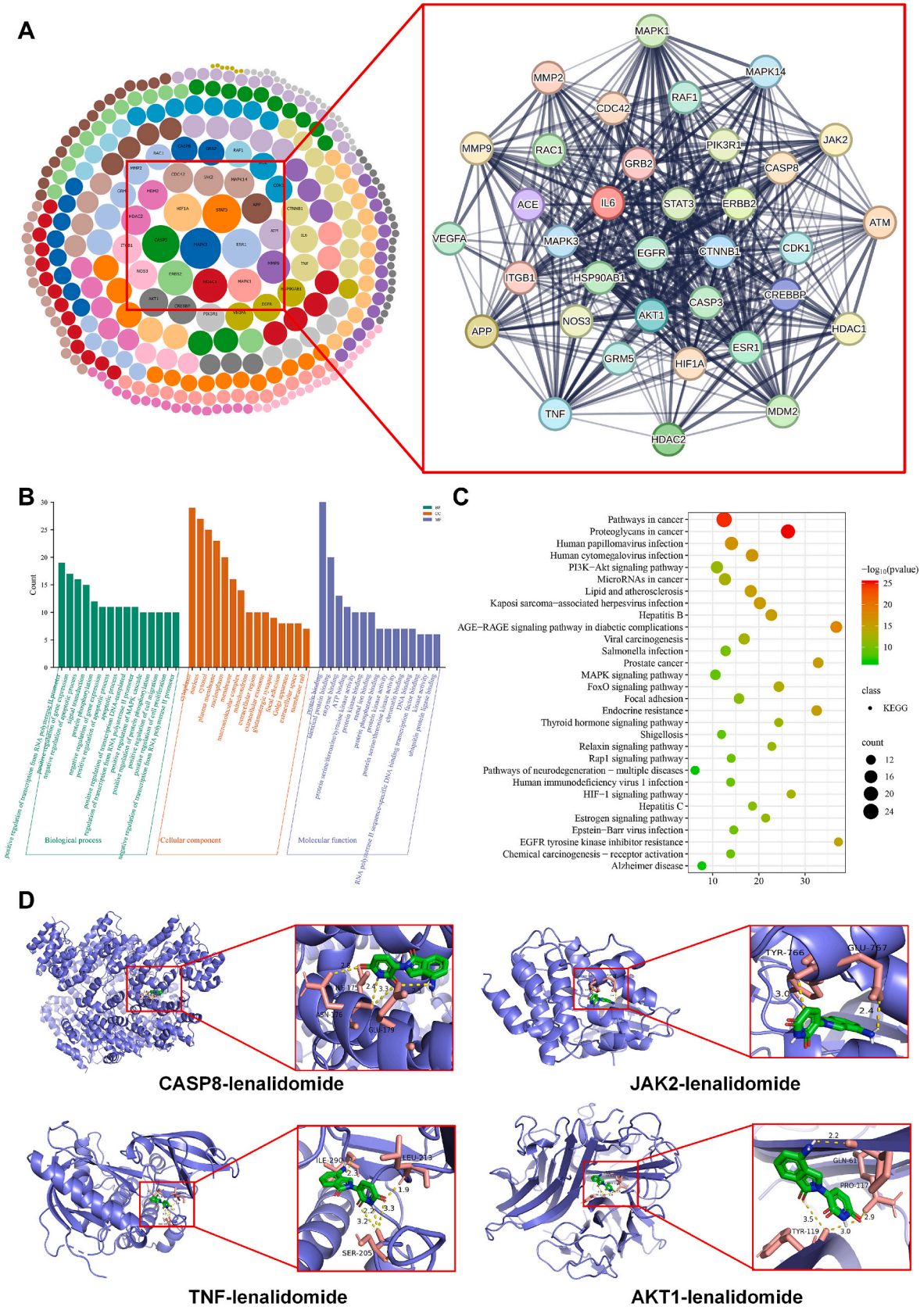

Fig. 7. Network pharmacology analysis. (A) The targets of lenalidomide and PPI network of melanoma-related targets of lenalidomide. (B) The top 35 targets involved in GO biological processes, molecular functions, and cell components. (C) KEGG analysis of the top 35 protein targets. (D) Molecular docking models of the four targets and lenalidomide.

biological processes, including positive regulation of gene expression, negative regulation of the apoptotic process, protein phosphorylation, and others (Fig. 7B). Additionally, they were linked to 79 molecular functions such as protein binding, identical protein binding, enzyme binding, ATP binding, and protein serine/threonine/ tyrosine kinase activity, covering 63 cellular components such as cytoplasm, nucleus and cytosol. In the KEGG analysis, the 35 protein targets were found to be involved in 148 pathways. Notably, we found that pathways such as the PI3K-Akt signaling pathway, VEGF signaling pathway, and TNF signaling pathway were associated with tumorigenesis (Fig. 7C). Based on *p*-adjust $\leq$0.05, the target proteins associated with melanoma survival were identified as CASP8, JAK2, TNF and AKT1 (Fig. S3). Notably, higher expression levels of CASP8, JAK2 and TNF were found to be correlated with improved survival probabilities, whereas lower expression of AKT1 was associated with better survival outcomes. The expression levels of targets shown in Fig. S2 are similar to them. The network pharmacology analysis provided the direction for follow-up exploration of the mechanisms in play. More importantly, molecular docking technology was used to investigate the interactions between lenalidomide and these four target proteins. Using a threshold of docking energy less than −6 as an indicator of favorable binding potential, it was observed that lenalidomide exhibited strong binding potential with these four target proteins (Table S2). The docking model is presented in Fig. 7D.

3.6. Transcriptome analysis of melanoma mice model

For RNA-Seq experiments, the closer the correlation coefficient is to 1, the higher the pattern similarity expressed between samples (Fig. S4). Principal component analysis (PCA) reduced the large amount of gene expression information contained in the sample to a few unrelated principal components for comparison between samples (Fig. S5). DESeq2 ($|LogFC| > 2$, *p*-value <0.05) was used for differential expression analysis. A total of 8743 DEGs (2046 upregulated and 6697 downregulated) were screened for differentially expressed genes between the Model group and the Control group (Fig. 8A). Genes clustered in the same cluster may have similar biological functions, which can be used to predict the function of unknown genes, the gene expression of the Model group and the Control group was significantly different (Fig. 8B). The Venn diagram showed 24,030 significantly different genes shared by the Model group and the Control group (Fig. S6). GO enrichment analysis contained 4023 biological processes (BP), 390 cellular components (CC), and 573 molecular functions (MF) as conformed screening criteria, with *p*-adjust $\leq$0.05. As shown in Fig. 8C, the main BPs were response to skin development, epidermis development, DNA replication, etc. The CCs were response to collagen-containing extracellular matrix, myofibril, centromeric region, etc. The MFs were response to metal ion transmembrane transporter activity, cell adhesion molecule binding, passive transmembrane transporter activity, etc. KEGG enrichment analysis contained 115 signaling pathways as conformed screening criteria, with *p*-adjust $\leq$0.05. As shown in Fig. 8D, the main signaling pathways were response to PI3K-Akt signaling pathway, extracellular matrix (ECM)-receptor interaction, Rap1 signaling pathway, etc. Combined with the results of network pharmacology analysis, PI3K-Akt signaling pathway was selected as the core signaling pathway to provide reference for subsequent experiments (Fig. 8E). The expression levels of the top 35 targets identified through network pharmacology in the transcriptome are illustrated in Fig. S7, which is similar to the target expression levels shown in Fig. S2. The relevant data of predicted core survival targets CASP8, JAK2, TNF, and AKT1 in DEGs are shown in Table S3. Based on Fig. S7 and Table S3, TNF and AKT1 are selected as core targets to provide reference for subsequence experiments.

3.7. The effect of lenalidomide on TNF-α and PI3K/AKT signaling pathway

To further explore whether lenalidomide regulated the TNF-α, and PI3K-AKT signaling pathways, the expression of relative proteins in tumor cells or in vivo tumors were detected. IF results demonstrated that Len-NBHs could effectively increase TNF-α expression in tumor tissues compared to the untreated control (Fig. 9A, B). This result contradicts most studies that show the TNF-α expression level in the tumor microenvironment decreases following drug treatment. A review of the relevant literature revealed that antitumor drugs in the early stages of clinical treatment increases TNF-α levels and promotes favorable immune responses [Aue et al., 2009]. This study aligns with our objective of developing Len-NBHs for surgical adjuvant therapy.

Following treatment of B16-F10 cells with varying concentrations of lenalidomide, cellular proteins were extracted and subjected to western blot analysis to assess the expression of the following target proteins: proteins related with the core targets of melanoma and PI3K/AKT signaling pathway, including AKT1, PI3K, p-AKT1, and p-PI3K. A dose-dependent reduction in p-PI3K and p-AKT in B16-F10 cells was noted (Fig. 9C, D). In addition, the in vivo experiments indicated that Len-NBHs reduced the expression of activated AKT and PI3K (Fig. 9E, F), thereby inhibiting the activation of the PI3K-AKT signaling pathway in tumor tissues and demonstrating its effectiveness in inhibiting tumor growth. To further investigate the gene-regulatory effects of Len-NBHs on melanoma, the relative mRNA expression of AKT1 and PI3K was significantly lower in the treatment group compared to the untreated group (Fig. 9G, H).

4. Discussion

Melanoma, a highly invasive and deadly form of skin cancer [Choi et al., 2023], is the subject of this study, which introduces an effective adjuvant administration method for regulating immune responses against malignant melanoma. Through literature research [Yao et al., 2023; Sato et al., 2015; Oktay et al., 2021; Thang et al., 2023; Mathiyalagan et al., 2022], we learned that nano-suspensions with small particle sizes can improve the rate of drug penetration through the skin, increase the accumulation of drugs in the skin, form a drug reservoir in the skin, enhance therapeutic effects, prolong action time, reduce the frequency of administration, and increase patient adherence to medication. In addition, hydrogels have viscosity, which can improve the retention time of drugs in the skin. Therefore, we chose to prepare lenalidomide as a nano-suspension and disperse it in a hydrogel matrix. We also confirmed through in vitro transdermal experiments that the rate of lenalidomide nano-hydrogel penetration through the skin and its accumulation in the skin are significantly higher than that of lenalidomide raw material. The ideal neoadjuvant therapy should not only reduce tumor volume but also activate anti-tumor immune responses to prevent recurrence. Immune checkpoint inhibitor (ICI) therapy is considered a promising innovation in melanoma treatment, but its clinical success rate varies. Some patients benefit from ICI treatment due to the induction of anti-tumor T cells before treatment. Successful activation of these anti-tumor T cells can enhance the efficacy of ICIs [Sambi et al., 2019; Backlund et al., 2023; Lai-Kwon et al., 2023; Augustin et al., 2023; Pavlick et al., 2023]. The study results demonstrate that Len-NBHs successfully inhibit the growth of subcutaneous B16-F10 tumor cells, meanwhile lenalidomide-treated B16-F10 cells exhibited arrest in the G1 phase of the cell cycle, leading to a block in cell proliferation. All Len-NBHs treatment groups in the experiment increased the expression of T cell markers CD8 and CD4, along with increased expression of CD86, CD80 and CD11c dendritic cell markers. These findings suggest that Len-NBHs may enhance the anti-tumor effect of ICI treatment, positioning percutaneous Len-NBHs as a promising pre-ICI supplemental treatment and a neoadjuvant therapy, reducing tumor volume and surgical area, thus mitigating the risk of tumor recurrence.

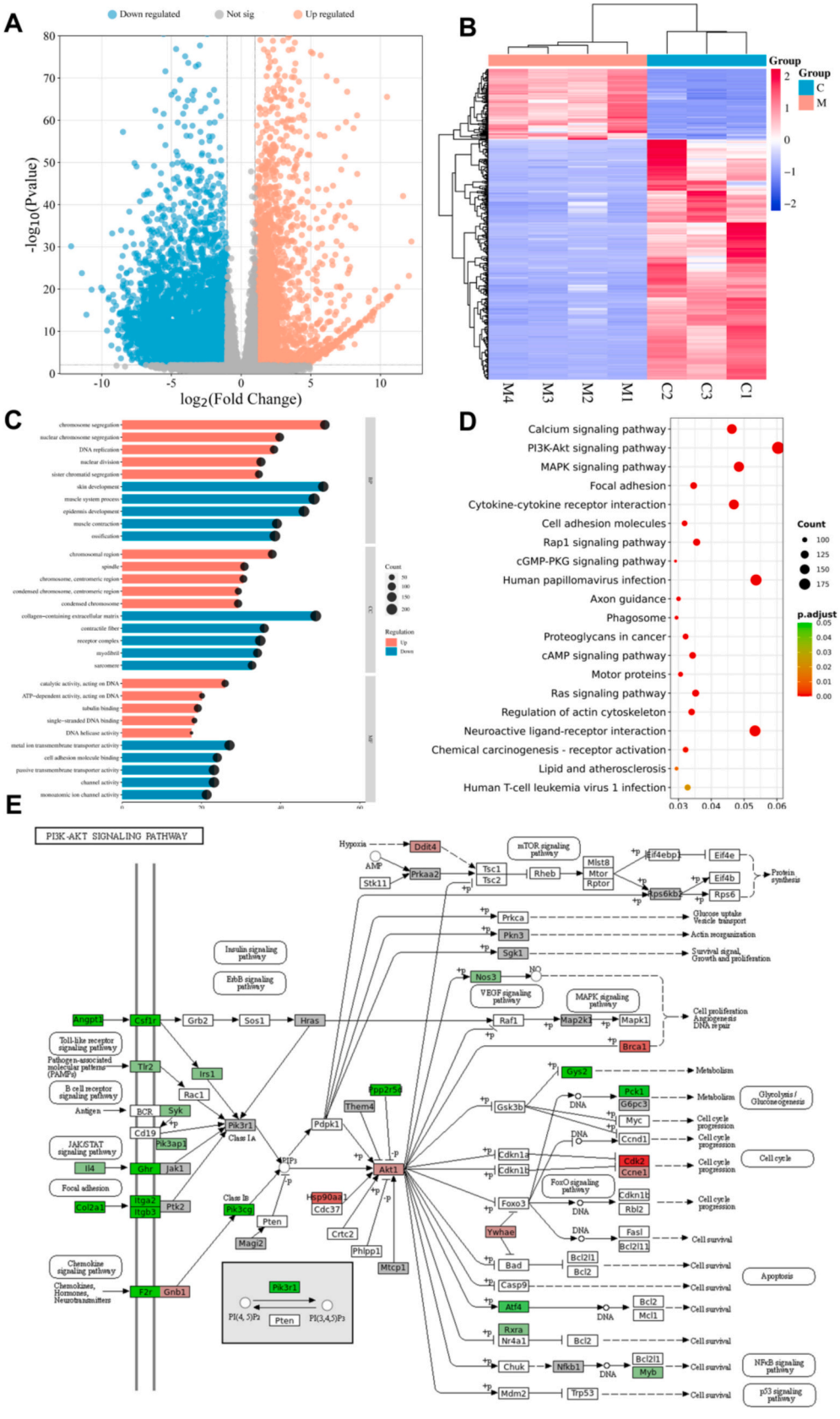

Fig. 8. Transcriptome analysis of melanoma mouse model. (A) Volcano plot of the differentially expressed genes. Blue indicates the down-regulated gene, and red indicates the up-regulated gene. (B) Cluster Analysis of the differentially expressed genes. Blue indicates low gene expression, red indicates high gene expression, and the connection represents the clustering result. (C) GO enrichment analysis, including BP, CC, and MF. (D) The top 20 KEGG analyses for signaling pathway. (E) PI3K/AKT signaling pathway. (For interpretation of the references to colour in this figure legend, the reader is referred to the web version of this article.)

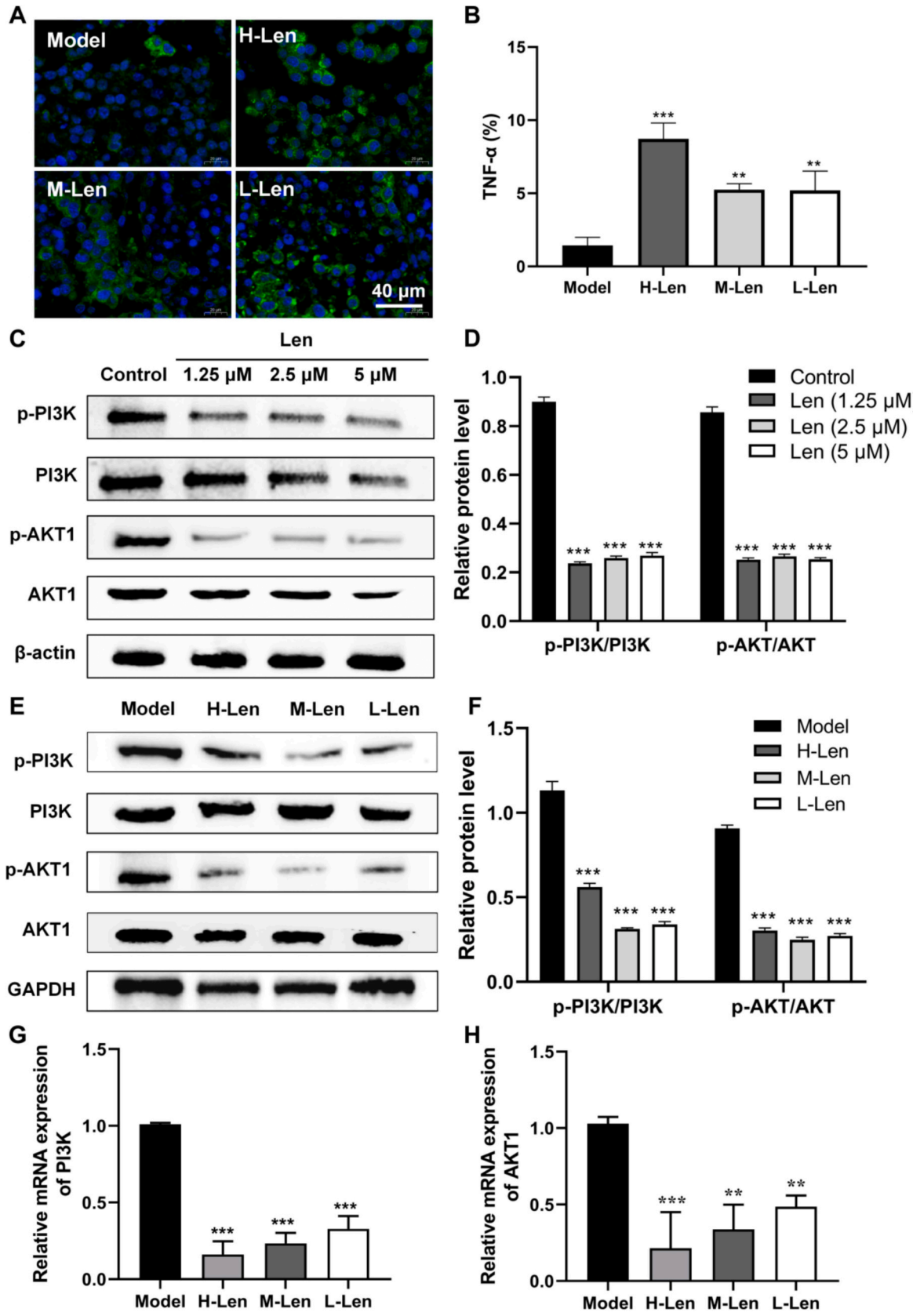

Fig. 9. Validation of predicted targets and assessment of the PI3K/AKT signaling pathway in melanoma. (A) The merged IF images of DAPI and TNF-α in tumor tissues (scale bar = 40 μm). (B) Quantitative analysis of expression of TNF-α in tumor tissues. (C) Western blotting of AKT1, PI3K, p-AKT1, and p-PI3K in B16-F10 cells. (D) Quantitative analysis of p-PI3K/PI3K, p-AKT1/AKT1 ratio in B16-F10 cells. (E) Western blotting of AKT1, PI3K, p-AKT1, and p-PI3K in tumor tissues. (F) Quantitative analysis of p-PI3K/PI3K, p-AKT1/AKT1 ratio in tumor tissues. (G, H) RT-qPCR was used to detect the relative mRNA expression of AKT1 and PI3K in each group of tumor tissues. $^{**}p < 0.01$, $^{***}p < 0.001$, vs the control group or model group.

Network pharmacology and transcriptomic analysis indicated that lenalidomide could affect the PI3K/AKT pathway by inhibiting the activation of key targets PI3K and AKT within the pathway, subsequently regulating the expression of upstream and downstream target proteins [Liu et al., 2023; Yang et al., 2023; Xiang et al., 2021; Gomez et al., 2022; Elia et al., 2018; Liu et al., 2021]. Activation of the PI3K/AKT pathway stimulates cell growth and proliferation. Overactivation of this signaling pathway can lead to abnormal cell proliferation and tumor formation. AKT, also known as protein kinase B, is a key regulator of various cellular processes, including growth, proliferation, migration, angiogenesis, and apoptosis [Li et al., 2023; Wang et al., 2022a]. Len-NBHs exhibit the ability to selectively bind to AKT within the skin barrier, thereby preventing its phosphorylation and, consequently, mitigating the excessive activation of the PI3K/AKT pathway within the tumor microenvironment (TME). Extracellular matrix (ECM) is a non-cellular component of the TME matrix and plays an important role in the development of cancer, immune cell recruitment and tissue metastasis. MMPs (such as MMP2, MMP9) are the main enzymes involved in ECM degradation. Protease-induced decomposition of ECM components is essential for tumor cells to cross the tissue barrier [Wang et al., 2022b]. CD93 is overexpressed in tumor vessels of many solid tumors, and studies have shown that VEGF directly regulates the expression of CD93. When VEGF is exposed to TME, CD93 is selectively up-regulated in the tumor vessels[Sun et al., 2021]. Epidermal growth factor receptor (EGFR) and vascular endothelial growth factor (VEGFA) have common downstream signaling pathways, represented by PI3K/AKT signaling pathway [Le et al., 2021; Pérez-Gutiérrez and Ferrara, 2023; Zhang et al., 2023; Liu et al., 2022; Eidizade et al., 2023; Rai and Shanker, 2024], which is related to angiogenesis, cell proliferation, growth, metastasis and adhesion. In our study, an interesting phenomenon was observed: the well-known inflammatory marker TNF-α showed an upward trend after treatment with Len-NBHs, which contradicts the general situation where TNF-α decreases in the tumor microenvironment after antitumor drug treatment. By reviewing the literature, we discovered that elevated TNF-α levels have also been observed in some similar tumor studies, typically during the early stages of treatment. After drug administration, the body enters a state of intense immune activation [Aue et al., 2009], leading to an increase in TNF-α levels. During the treatment process, TNF-α levels gradually decrease. Moreover, numerous studies have shown that TNF-α has a dual role in tumor cells. It can both promote tumor growth and metastasis and induce tumor cell apoptosis, while also enhancing anti-tumor immune responses [Wang and Lin, 2008; Bertazza and Mocellin, 2010]. In addition, we used a small number of tumor model mice and extended the administration time. After 30 days of treatment, serum was collected for testing, revealing a decreasing trend in TNF-α (Fig. S8). However, since our research aim is to use the Len-NBHs for preoperative local administration to inhibit the spread of melanoma, thereby reducing the extent of surgery while broadly activating the immune system to improve patient prognosis, an extended administration time does not align with our research objectives. We will conduct more in-depth exploration of lenalidomide in the future.

5. Conclusion

In summary, the mechanism behind this inhibition of malignant melanoma growth can be summarized as follows: (1) Len-NBHs affect the cell cycle and tumor angiogenesis, leading to tumor cell apoptosis; (2) Len-NBHs induce the release of cytokines within the tumor microenvironment, attracting immune cells to the site; (3) Len-NBHs effectively activate multiple subsets of skin dendritic cells simultaneously, triggering a broader immune response; (4) Len-NBHs influence the PI3K/AKT pathway and its upstream and downstream molecules, altering the tumor microenvironment. Preoperative administration of Len-NBHs can inhibit the outward spread of melanoma, reduce tumor size, thereby decreasing the surgical excision area and improving patient survival rates and prognosis. This study offers a promising clinical adjuvant therapy for the treatment of skin-related cancers. Future research may involve further optimizing the formulation of Len-NBHs to enhance their transdermal efficiency and conduct clinical research with human subjects on the premise of ensuring the safety of the preparation.

Funding information

This work was supported by the Basic Science Research Program from Air Force Medical University of China (No.2022LC2203, and No. 2019ZFC005).

Ethics statement

All experimental protocols with mice followed the ARRIVE guidelines (Animal Research: Reporting of In Vivo Experiments) and were approved by the Ethics Committee of the Air Force Medical Center (Ethical approval number: 2023–31-PJ01).

CRediT authorship contribution statement

Mengdi Zhang: Writing – original draft, Visualization, Validation, Resources, Project administration, Methodology, Investigation, Formal analysis, Data curation, Conceptualization. **Haiying Qiu:** Writing – review & editing, Visualization, Validation, Resources, Data curation, Conceptualization. **Zheyi Han:** Resources, Data curation. **Yazhong Ma:** Software, Formal analysis. **Jingjing Hou:** Supervision, Formal analysis, Conceptualization. **Jingwei Yuan:** Resources, Data curation. **Haiyan Jia:** Software, Formal analysis. **Menglu Zhou:** Supervision, Investigation. **Hongjie Lu:** Visualization, Validation. **Yan Wu:** Writing – review & editing, Supervision, Funding acquisition.

Declaration of competing interest

The authors declare that they have no known competing financial interests or personal relationships that could have appeared to influence the work reported in this paper.

Data availability

Data will be made available on request.

Acknowledgments

Thank to ZYEdit for language editing.

Appendix A. Supplementary data

Supplementary data to this article can be found online at https://doi.org/10.1016/j.ijpx.2025.100316.

References

Amberger, J.S., Bocchini, C.A., Schiettecatte, F., Scott, A.F., Hamosh, A., 2015. OMIM.org: Online Mendelian Inheritance in Man (OMIM®), an online catalog of human genes and genetic disorders. Nucleic Acids Res. 43, D789–D887.

Aue, G., Njuguna, N., Tian, X., Soto, S., Hughes, T., Vire, B., Keyvanfar, K., Gibellini, F., Valdez, J., Boss, C., Samsel, L., McCoy Jr., J.P., Wilson, W.H., Pittaluga, S., Wiestner, A., 2009. Lenalidomide-induced upregulation of CD80 on tumor cells correlates with T-cell activation, the rapid onset of a cytokine release syndrome and leukemic cell clearance in chronic lymphocytic leukemia. Haematologica 94, 1266–1273.

Augustin, R.C., Newman, S., Li, A., Joy, M., Lyons, M., Pham, M.P., Lucas, P., Smith, K., Sander, C., Isett, B., Davar, D., Najjar, Y.G., Zarour, H.M., Kirkwood, J.M., Luke, J.J., Bao, R., 2023. Identification of tumor-intrinsic drivers of immune exclusion in acral melanoma. J. Immunother. Cancer 11, e007567.

Backlund, E., Grozman, V., Egyhazi Brage, S., Lewensohn, R., Lindberg, K., Helgadottir, H., 2023. Radiotherapy with or without immunotherapy in metastatic melanoma: efficacy and tolerability. Acta Oncol. 62, 1921–1930.

Bertazza, L., Mocellin, S., 2010. The dual role of tumor necrosis factor (TNF) in cancer biology. Curr. Med. Chem. 17, 3337–3352.
Carr, S., Smith, C., Wernberg, J., 2020. Epidemiology and risk factors of melanoma. Surg. Clin. North Am. 100, 1–12.
Chandrashekar, D.S., Karthikeyan, S.K., Korla, P.K., Patel, H., Shovon, A.R., Athar, M., Netto, G.J., Qin, Z.S., Kumar, S., Manne, U., Creighton, C.J., Varambally, S., 2022. UALCAN: an update to the integrated cancer data analysis platform. Neoplasia 25, 18–27.
Chen, C.H., Weng, T.H., Chuang, C.H., Huang, K.Y., Huang, S.C., Chen, P.R., Huang, H. H., Huang, L.Y., Shen, P.C., Chuang, P.Y., Huang, H.Y., Wu, Y.S., Chang, H.C., Weng, S.L., Liao, K.W., 2023. Transdermal nanolipoplex simultaneously inhibits subcutaneous melanoma growth and suppresses systemically metastatic melanoma by activating host immunity. Nanomedicine 47, 102628.
Chen, T., Liu, Y.X., Chen, T., Yang, M., Fan, S., Shi, M., Wei, B., Lv, H., Cao, W., Wang, C., Cui, J., Zhao, J., Han, Y., Xi, J., Zheng, Z., Huang, L., 2024. ImageGP 2 for enhanced data visualization and reproducible analysis in biomedical research. Imeta 3, e239.
Choi, Y., Son, W., Han, Y., Chae, J., Yang, C.S., Choi, J., 2023. Glycan targeting nanoparticle for photodynamic immunotherapy of melanoma. Acta Pharm. Sin. B 13, 1903–1918.
Daina, A., Michielin, O., Zoete, V., 2019. SwissTargetPrediction: updated data and new features for efficient prediction of protein targets of small molecules. Nucleic Acids Res. 47, W357–W364.
Davis, L.E., Shalin, S.C., Tackett, A.J., 2019. Current state of melanoma diagnosis and treatment. Cancer Biol. Ther. 20, 1366–1379.
Davis, A.P., Wiegers, T.C., Johnson, R.J., Sciaky, D., Wiegers, J., Mattingly, C.J., 2023. Comparative Toxicogenomics Database (CTD): update 2023. Nucleic Acids Res. 51, D1257–D1262.
Domingues, B., Lopes, J.M., Soares, P., Populo, H., 2018. Melanoma treatment in review. Immunotargets Ther 7, 35–49.
Eberhardt, J., Santos-Martins, D., Tillack, A.F., Forli, S., 2021. AutoDock Vina 1.2.0: new docking methods, expanded force field, and Python bindings. J. Chem. Inf. Model. 61, 3891–3898.
Eidizade, F., Soukhtanloo, M., Zhiani, R., Mehrzad, J., Mirzavi, F., 2023. Inhibition of glioblastoma proliferation, invasion, and migration by Urolithin B through inducing G0/G1 arrest and targeting MMP-2/−9 expression and activity. Biofactors 49, 379–389.
Elia, A.R., Grioni, M., Basso, V., Curnis, F., Freschi, M., Corti, A., Mondino, A., Bellone, M., 2018. Targeting tumor vasculature with TNF leads effector T cells to the tumor and enhances therapeutic efficacy of immune checkpoint blockers in combination with adoptive cell therapy. Clin. Cancer Res. 24, 2171–2181.
Fuchs, O., 2019. Treatment of lymphoid and myeloid malignancies by immunomodulatory drugs. Cardiovasc. Hematol. Disord. Drug Targets 19, 51–78.
Gandhi, A.K., Kang, J., Havens, C.G., Conklin, T., Ning, Y., Wu, L., Ito, T., Ando, H., Waldman, M.F., Thakurta, A., Klippel, A., Handa, H., Daniel TO, Schafer, P.H., Chopra, R., 2014. Immunomodulatory agents lenalidomide and pomalidomide co-stimulate T cells by inducing degradation of T cell repressors Ikaros and Aiolos via modulation of the E3 ubiquitin ligase complex CRL4(CRBN). Br. J. Haematol. 164, 811–832.
Gomez, G.V.B., Lourenço, G.J., Monteiro, L.M.O., Rocha, R.S., Fernández, K.A.M., Recio, J.A., Torricelli, C., Coser, L.O., Oliveira, A.L.R., Carron, J., Moraes, A.M., Lima, C.S.P., 2022. Association of JAK/STAT genetic variants with cutaneous melanoma. Front. Oncol. 12, 943483.
Gordon, R., 2013. Skin cancer: an overview of epidemiology and risk factors. Semin. Oncol. Nurs. 29, 160–169.
Hagner, P.R., Chiu, H., Ortiz, M., Apollonio, B., Wang, M., Couto, S., Waldman, M.F., Flynt, E., Ramsay, A.G., Trotter, M., Gandhi, A.K., Chopra, R., Thakurta, A., 2017. Activity of lenalidomide in mantle cell lymphoma can be explained by NK cell-mediated cytotoxicity. Br. J. Haematol. 179, 399–409.
Hetland, G., Johnson, E., Lyberg, T., Kvalheim, G., 2011. The mushroom agaricus blazei murill elicits medicinal effects on tumor, infection, allergy, and inflammation through its modulation of innate immunity and amelioration of Th1/Th2 imbalance and inflammation. Adv. Pharmacol. Sci. 2011, 157015.
Hideshima, T., Ogiya, D., Liu, J., Harada, T., Kurata, K., Bae, J., Massefski, W., Anderson, K.C., 2021. Immunomodulatory drugs activate NK cells via both Zap-70 and cereblon-dependent pathways. Leukemia 35, 177–188.
Hossain, S.M., Eccles, M.R., 2023. Phenotype switching and the melanoma microenvironment; impact on immunotherapy and drug resistance. Int. J. Mol. Sci. 24, 1601.
Hou, J.J., Qiu, H.Y., Wang, W.M., An, F., Wu, Y., 2023. Study on preparation of lenalidomidenano hydrogeland transdermal absorption in vitro. Chinese J. Hosp. Pharm. 43, 2243–2247.
Jia, H.Y., Qiu, H.Y., Zhang, M.D., Hou, J.J., Zhou, M.L., Wu, Y., 2022. Lenalidomide attenuates IMQ-induced inflammation in a mouse model of psoriasis. Biomed. Pharmacother. 156, 113883.
Knox, C., Wilson, M., Klinger, C.M., Franklin, M., Oler, E., Wilson, A., Pon, A., Cox, J., Chin, N.E.L., Strawbridge, S.A., Garcia-Patino, M., Kruger, R., Sivakumaran, A., Sanford, S., Doshi, R., Khetarpal, N., Fatokun, O., Doucet, D., Zubkowski, A., Rayat, D.Y., Jackson, H., Harford, K., Anjum, A., Zakir, M., Wang, F., Tian, S., Lee, B., Liigand, J., Peters, H., Wang, R.Q.R., Nguyen, T., So, D., Sharp, M., da Silva, R., Gabriel, C., Scantlebury, J., Jasinski, M., Ackerman, D., Jewison, T., Sajed, T., Gautam, V., Wishart, D.S., 2024. DrugBank 6.0: the DrugBank knowledgebase for 2024. Nucleic Acids Res. 52, D1265–D1275.
Krämer, I., Engelhardt, M., Fichtner, S., Neuber, B., Medenhoff, S., Bertsch, U., Hillengass, J., Raab, M.S., Hose, D., Ho, A.D., Goldschmidt, H., Hundemer, M., 2016. Lenalidomide enhances myeloma-specific T-cell responses in vivo and in vitro. Oncoimmunology 5, e1139662.
Lai-Kwon, J., Inderjeeth, A.J., Lisy, K., Sandhu, S., Rutherford, C., Jefford, M., 2023. Impact of immune checkpoint inhibitors and targeted therapy on health-related quality of life of people with stage III and IV melanoma: a mixed-methods systematic review. Eur. J. Cancer 184, 83–105.
Le, X., Nilsson, M., Goldman, J., Reck, M., Nakagawa, K., Kato, T., Ares, L.P., Frimodt-Moller, B., Wolff, K., Visseren-Grul, C., Heymach, J.V., Garon, E.B., 2021. Dual EGFR-VEGF pathway inhibition: a promising strategy for patients with EGFR-mutant NSCLC. J. Thorac. Oncol. 16, 205–215.
Li, C., Chen, B., Zhang, J., Yang, J., Guo, M., Ren, Y., Zhou, Z., Fung, K.M., Li, M., Zhang, L., Liu, Z., 2023. SEM1 promotes tumor progression of glioblastoma via activating the akt signaling pathway. Cancer Lett. 577, 216368.
Liu, H., Amakye, W.K., Ren, J., 2021. Codonopsis pilosula polysaccharide in synergy with dacarbazine inhibits mouse melanoma by repolarizing M2-like tumor-associated macrophages into M1-like tumor-associated macrophages. Biomed. Pharmacother. 142, 112016.
Liu, J., Chen, T., Li, S., Liu, W., Wang, P., Shang, G., 2022. Targeting matrix metalloproteinases by E3 ubiquitin ligases as a way to regulate the tumor microenvironment for cancer therapy. Semin. Cancer Biol. 86, 259–268.
Liu, T., Xiang, W., Chen, Z., Wang, G., Cao, R., Zhou, F., Meng, Z., Luo, Y., Chen, L., 2023. Hypoxia-induced PLOD2 promotes clear cell renal cell carcinoma progression via modulating EGFR-dependent AKT pathway activation. Cell Death Dis. 14, 774.
Marriott, J.B., Clarke, I.A., Dredge, K., Muller, G., Stirling, D., Dalgleish, A.G., 2002. Thalidomide and its analogues have distinct and opposing effects on TNF-alpha and TNFR2 during co-stimulation of both CD4(+) and CD8(+) T cells. Clin. Exp. Immunol. 130, 75–84.
Mathiyalagan, R., Kariyarath Valappil, A., Yang, D.C., Kang, S.C., Thambi, T., 2022. Gene Regulations upon Hydrogel-Mediated Drug delivery Systems in Skin Cancers-An Overview. Gels 8, 560.
Oktay, A.N., Ilbasmis-Tamer, S., Uludag, O., Celebi, N., 2021. Enhanced dermal delivery of flurbiprofen nanosuspension based gel: development and ex vivo permeation, pharmacokinetic evaluations. Pharm. Res. 38, 991–1009.
Patel, H., Yacoub, N., Mishra, R., White, A., Long, Y., Alanazi, S., Garrett, J.T., 2020. Current advances in the treatment of BRAF-mutant melanoma. Cancers (Basel) 12, 482.
Pavlick, A.C., Ariyan, C.E., Buchbinder, E.I., Davar, D., Gibney, G.T., Hamid, O., Hieken, T.J., Izar, B., Johnson, D.B., Kulkarni, R.P., Luke, J.J., Mitchell, T.C., Mooradian, M.J., Rubin, K.M., Salama, A.K., Shirai, K., Taube, J.M., Tawbi, H.A., Tolley, J.K., Valdueza, C., Weiss, S.A., Wong, M.K., Sullivan, R.J., 2023. Society for Immunotherapy of Cancer (SITC) clinical practice guideline on immunotherapy for the treatment of melanoma, version 3.0. J. Immunother. Cancer 11, e006947.
Pérez-Gutiérrez, L., Ferrara, N., 2023. Biology and therapeutic targeting of vascular endothelial growth factor a. Nat. Rev. Mol. Cell Biol. 24, 816–834.
Piñero, J., Ramírez-Anguita, J.M., Saüch-Pitarch, J., Ronzano, F., Centeno, E., Sanz, F., Furlong, L.I., 2020. The DisGeNET knowledge platform for disease genomics: 2019 update. Nucleic Acids Res. 48, D845–D855.
Rai, G.P., Shanker, A., 2024. Coevolution-based computational approach to detect resistance mechanism of epidermal growth factor receptor. Biochim. Biophys. Acta, Mol. Cell Res. 1871, 119592.
Rappaport, N., Twik, M., Plaschkes, I., Nudel, R., Iny Stein, T., Levitt, J., Gershoni, M., Morrey, C.P., Safran, M., Lancet, D., 2017. MalaCards: an amalgamated human disease compendium with diverse clinical and genetic annotation and structured search. Nucleic Acids Res. 45, D877–D887.
Sambi, M., Bagheri, L., Szewczuk, M.R., 2019. Current challenges in cancer immunotherapy: multimodal approaches to improve efficacy and patient response rates. J. Oncol. 2019, 4508794.
Sato, T., Takeuchi, H., Sakurai, T., Tanaka, K., Matsuki, K., Higashi, K., Moribe, K., Yamamoto, K., 2015. Characterization of a riboflavin non-aqueous nanosuspension prepared by bead milling for cutaneous application. Chem Pharm Bull (Tokyo). 63, 88–94.
Schadendorf, D., van Akkooi, A.C.J., Berking, C., Griewank, K.G., Gutzmer, R., Hauschild, A., Stang, A., Roesch, A., Ugurel, S., 2018. Melanoma. Lancet 392, 971–984.
Semeraro, M., Vacchelli, E., Eggermont, A., Galon, J., Zitvogel, L., Kroemer, G., Galluzzi, L., 2013. Trial watch: lenalidomide-based immunochemotherapy. Oncoimmunology 2, e26494.
Sherman, B.T., Hao, M., Qiu, J., Jiao, X., Baseler, M.W., Lane, H.C., Imamichi, T., Chang, W., 2022. DAVID: a web server for functional enrichment analysis and functional annotation of gene lists (2021 update). Nucleic Acids Res. 50, W216–W221.
Stelzer, G., Rosen, N., Plaschkes, I., Zimmerman, S., Twik, M., Fishilevich, S., Stein, T.I., Nudel, R., Lieder, I., Mazor, Y., Kaplan, S., Dahary, D., Warshawsky, D., Guan-Golan, Y., Kohn, A., Rappaport, N., Safran, M., Lancet, D., 2016. The GeneCards suite: from gene data mining to disease genome sequence analyses. Curr. Protoc. Bioinformatics 54, 1.30.1–1.30.33.
Stewart, A.K., 2014. Medicine. How thalidomide works against cancer. Science 343, 256–263.
Sun, Y., Chen, W., Torphy, R.J., Yao, S., Zhu, G., Lin, R., Lugano, R., Miller, E.N., Fujiwara, Y., Bian, L., Zheng, L., Anand, S., Gao, F., Zhang, W., Ferrara, S.E., Goodspeed, A.E., Dimberg, A., Wang, X.J., Edil, B.H., Barnett, C.C., Schulick, R.D., Chen, L., Zhu, Y., 2021. Blockade of the CD93 pathway normalizes tumor vasculature to facilitate drug delivery and immunotherapy. Sci. Transl. Med. 13, eabc8922.
Szklarczyk, D., Santos, A., von Mering, C., Jensen, L.J., Bork, P., Kuhn, M., 2016. STITCH 5: augmenting protein-chemical interaction networks with tissue and affinity data. Nucleic Acids Res. 44, D380–D384.

Szklarczyk, D., Kirsch, R., Koutrouli, M., Nastou, K., Mehryary, F., Hachilif, R., Gable, A. L., Fang, T., Doncheva, N.T., Pyysalo, S., Bork, P., Jensen, L.J., von Mering, C., 2023. The STRING database in 2023: protein-protein association networks and functional enrichment analyses for any sequenced genome of interest. Nucleic Acids Res. 51, D638–D646.

Thang, N.H., Chien, T.B., Cuong, D.X., 2023. Polymer-based hydrogels applied in drug delivery: an overview. Gels 9, 523.

Wang, X., Lin, Y., 2008. Tumor necrosis factor and cancer, buddies or foes? Acta Pharmacol. Sin. 29, 1275–1363.

Wang, X., Shen, Y., Wang, S., Li, S., Zhang, W., Liu, X., Lai, L., Pei, J., Li, H., 2017. PharmMapper 2017 update: a web server for potential drug target identification with a comprehensive target pharmacophore database. Nucleic Acids Res. 45, W356–W360.

Wang, J., Hu, K., Cai, X., Yang, B., He, Q., Wang, J., Weng, Q., 2022a. Targeting PI3K/AKT signaling for treatment of idiopathic pulmonary fibrosis. Acta Pharm. Sin. B 12, 18–32.

Wang, Q., Wang, K., Tan, X., Li, Z., Wang, H., 2022b. Immunomodulatory role of metalloproteases in cancers: current progress and future trends. Front. Immunol. 13, 1064033.

Whirl-Carrillo, M., Huddart, R., Gong, L., Sangkuhl, K., Thorn, C.F., Whaley, R., Klein, T. E., 2021. An evidence-based framework for evaluating pharmacogenomics knowledge for personalized medicine. Clin. Pharmacol. Ther. 110, 563–572.

Xi, P., Niu, Y., Zhang, Y., Li, W., Gao, F., Gu, W., Kui, F., Liu, Z., Lu, L., Du, G., 2022. The mechanism of dioscin preventing lung cancer based on network pharmacology and experimental validation. J. Ethnopharmacol. 292, 115138.

Xiang, Y.K., Peng, F.H., Guo, Y.Q., Ge, H., Cai, S.Y., Fan, L.X., Peng, Y.X., Wen, H., Wang, Q., Tao, L., 2021. Connexin32 activates necroptosis through Src-mediated inhibition of caspase 8 in hepatocellular carcinoma. Cancer Sci. 112, 3507–3519.

Yang, Y., Ma, S., Ye, Z., Zheng, Y., Zheng, Z., Liu, X., Zhou, X., 2023. Oncogenic DNA methyltransferase 1 activates the PI3K/AKT/mTOR signalling by blocking the binding of HSPB8 and BAG3 in melanoma. Epigenetics 18, 2239607.

Yao, S., Chen, N., Sun, X., Wang, Q., Li, M., Chen, Y., 2023. Size-dependence of the skin penetration of andrographolide nanosuspensions: in vitro release-ex vivo permeation correlation and visualization of the delivery pathway. Int. J. Pharm. 641.

Zhang, L., Qian, Z., Cai, Z., Sun, L., Wang, H., Bartlett, J.B., Yi, Q., Wang, M., 2009. Synergistic antitumor effects of lenalidomide and rituximab on mantle cell lymphoma in vitro and in vivo. Am. J. Hematol. 84, 553–562.

Zhang, H., Zhou, J., Li, J., Wang, Z., Chen, Z., Lv, Z., Ge, L., Xie, G., Deng, G., Rui, Y., Huang, H., Chen, L., Wang, H., 2023. N6-methyladenosine promotes translation of VEGFA to accelerate angiogenesis in lung cancer. Cancer Res. 83, 2208–2225.

Zhao, T., Wang, Z., 2022. GraphBio: a shiny web app to easily perform popular visualization analysis for omics data. Front. Genet. 13, 957317.

Zhou, Y., Zhang, Y., Zhao, D., Yu, X., Shen, X., Zhou, Y., Wang, S., Qiu, Y., Chen, Y., Zhu, F., 2024. TTD: therapeutic target database describing target druggability information. Nucleic Acids Res. 52, D1465–D1477.